Available online at www.sciencedirect.com
ScienceDirect
International Journal of Mass Spectrometry 261 (2007) 227–233
International Journal of Mass Spectrometry
www.elsevier.com/locate/ijms

Photoionization and dissociative photoionization of the allyl radical, C_3H_5

Ingo Fischer [a,*], Thomas Schüßler [a], Hans-Jürgen Deyerl [b], Mohamed Elhanine [c], Christian Alcaraz [d,**]

[a] *Universität Würzburg, Institut für Physikalische Chemie, Am Hubland, D-97074 Würzburg, Germany*
[b] *Faculty of Natural Science, TU Chemnitz, D-09107 Chemnitz, Germany*
[c] *Laboratoire Francis Perrin, SPAM, CEA/Saclay, F-91191 Gif-sur-Yvette, France*
[d] *Laboratoire Chimie–Physique, Bât. 349, Centre Universitaire Paris-Sud, F-91405 Orsay Cedex, France*

Received 31 July 2006; received in revised form 16 September 2006; accepted 18 September 2006
Available online 13 October 2006

Abstract

The photoionization and dissociative photoionization of the allyl radical in the VUV range was investigated using synchrotron radiation. Allyl radicals were generated by flash pyrolysis from allyl iodide and 1,5-hexadiene. Mass spectra show the appearance of $C_3H_3^+$ as a fragment in the dissociative photoionization of allyl above 10 eV. Between 10.4 and 10.5 eV the $C_3H_3^+$ signal reaches 50% of its maximum value. Cyclopropenyl cation, c-$C_3H_3^+$, is the thermochemically most stable product, but accompanying ab initio computations indicate that formation of linear l-$C_3H_3^+$ becomes competitive at small excess energies. The dissociative photoionization of the precursor molecules is discussed as well. An ionization energy of 8.13 ± 0.01 eV was deduced from threshold photoelectron spectra.

Keywords: Hydrocarbon radicals; Allyl cation; Dissociative photoionization; Threshold photoelectron spectroscopy; Synchrotron radiation

1. Introduction

Investigations of the spectroscopy and dynamics of hydrocarbon radicals are motivated by their role as intermediates in reactive environments like combustion engines, the atmosphere or interstellar space. A large part of the chemistry of those systems is often determined by the dynamics of a few key radical species, thus considerable effort is devoted to a detailed understanding of gas phase radical chemistry. Whenever high energy radiation is present, i.e., in the upper atmosphere or in space, ions are readily formed that can participate in ion–molecule chemistry. The structure, energetics and reactivity of such ions has to be investigated in the laboratory to improve our understanding of the ion–molecule chemistry in reactive environments. An example of present interest is the possible contribution of cations of hydrocarbon radicals to the chemistry of the ionosphere of Titan, Saturn's larger moon [1,2], which is currently investigated by the ESA-NASA CASSINI-HUYGENS mission [3,4]. In recent ion mass spectra a large number of hydrocarbons $C_mH_n^+$ with $m \leq 7$ was identified [5]. A second example is the investigation of combustion processes: The detection of radicals by VUV spectroscopy was recently demonstrated to be a powerful diagnostic tool for elucidating the combustion dynamics [6–8]. However, this requires some knowledge of the species of interest beforehand. Due to the limited tuning range of VUV lasers, experiments are often carried out at synchrotron radiation (SR) facilities. However, a challenge in the research on reactive intermediates is the clean generation at high number densities. Since synchrotron light is not easily combined with radical sources that are mostly operated in a pulsed mode, only few reactive species have been studied [9–18]. In addition experiments using VUV lamps were performed [19–22], but for most species only photoionization efficiency (PIE) curves have been reported. In recent work on propargyl and ethyl [23] we showed that the VUV-photochemistry of radicals generated by flash pyrolysis can be investigated by threshold photoelectron photoion coincidence (TPEPICO [24]). Due to the additional energy information available from the photoelectron spectrum this technique is much better suited to investigate the chemistry of molecular ions than simple PIE spectroscopy.

* Corresponding author. Tel.: +49 931 888 6360; fax: +49 931 888 6362.
** Corresponding author. Tel.: +33 1 6915 7567; fax: +33 1 6915 6188.
E-mail addresses: ingo@phys-chemie.uni-wuerzburg.de (I. Fischer), christian.alcaraz@lcp.u-psud.fr (C. Alcaraz).

1387-3806/$ – see front matter © 2006 Elsevier B.V. All rights reserved.
doi:10.1016/j.ijms.2006.09.023

Allyl itself is an important intermediate in propane, butane or acetylene-rich flames and might play a role as an intermediate in tropospheric [25] or interstellar chemistry [26]. In an earlier communication [14] we reported a threshold photoelectron spectrum and investigated the onset of dissociative photoionization using TPEPICO. In the present paper we want to give a more detailed account and discuss the work in the light of supporting computational studies.

2. Experimental

The experiments were carried out at the Super-ACO storage ring at LURE in Orsay, using the SAPHIRS setup [27] at the SU 5 crossed undulator beamline [28], which provides tunable radiation between 5 and 40 eV. The wavelength was selected by a 6.65 m normal incidence monochromator. A photon flux of more than 10^{10} photons/s is available in this range in a bandwidth of $\lambda/\Delta\lambda = 50{,}000$. Higher harmonics originating from second order diffraction of the grating were eliminated by a gas filter operated with Ar. Both modes provided by Super-ACO, a 24-bunch mode with pulses every 10 ns and a two-bunch mode with pulses separated by 120 ns, were employed in the experiments. The photon energy was monitored during the experiments by recording the fluorescence from a sodium salicylate-coated window mounted at the exit window of the experimental setup.

The SAPHIRS apparatus [27] is equipped with two time-of-flight spectrometers, one for ion detection and one for electron detection, and specifically designed to study the ionization and dissociative ionization of molecules cooled in a supersonic molecular beam using threshold photoelectron–photoion coincidences. Threshold electrons are extracted by a static electric field of 0.8 V/cm through an aperture of 2 mm diameter that provides a geometric discrimination of energetic electrons [24]. In two-bunch mode kinetic electrons moving on the axis of the electron analyzer are temporally discriminated by limiting the electron detection to a 5 ns time gate. Using both geometrical and time discrimination threshold electrons can be detected with a resolution close to 10 meV (FWHM). In 24-bunch mode, on the other hand, the time gate cannot be used and detection of axial kinetic electrons cannot be completely suppressed. Since this leads to a tail in the transmission function of the electron analyzer that extends to higher kinetic energies [27], spectra recorded in this mode yield data with a less defined internal energy. The arrival of a threshold electron at the detector triggers the extraction of the ions in a Wiley–McLaren type time-of-flight mass spectrometer with two accelerating electric fields of 54 and 165 V/cm. Note that in all experiments discussed below only ions detected in coincidence with a threshold electron appear in the mass spectra. In threshold photoelectron (TPE) and ion yield spectra, the photon energy was scanned over the ionization threshold in either 2 or 3 meV steps, in the dissociative photoionization experiments a 50–100 meV step size was chosen. When a threshold electron and an ion are produced by synchrotron bunches within the same extraction pulse but originate from different molecules, false coincidences are detected. In order to correct the TPEPICO spectra for such false coincidences we used the following procedure: Recording of a mass spectrum was started by a random trigger signal rather than an electron, thus all ions detected correspond exclusively to accidental coincidences. This procedure yields the number of false coincidences per start signal, which is subsequently subtracted from the TPEPICO signal. However, as will be discussed below, it is possible that not all false coincidence are properly accounted for.

The flash pyrolysis source for radical generation is described in the literature [29]. A SiC tube fitted with two electrodes is mounted onto the faceplate of a solenoid valve (general valve). The precursors, allyl iodide (C_3H_5I) and hexadiene (C_6H_{10}), were obtained commercially from Fluka and used without further purification. They were seeded in 1 bar of Ar or He, and expanded through the SiC tube. The heating current was adjusted for optimal conversion of the precursors to allyl radicals. In most experiments described below, the valve was used with a nozzle of 0.5 mm orifice and triggered at a rate of 110 Hz. We adjusted the driving voltages for the solenoid valve in a way that the maximum signal was obtained. The pulsed valve is approximately open for about 50% of the time between two pulses and thus almost in a continuous mode. In other experiments a 0.1 mm nozzle was employed and the source ran continuously. Pulsed and continuous mode yielded similar spectra with comparable signal to noise ratio. To verify that given peaks originate from pyrolysis products rather than the precursor itself, control experiments with the pyrolysis source turned off were carried out.

3. Computational details

To aid the analysis of our experimental data the unimolecular reaction pathway of the allyl cation to cyclopropenyl cation, c-$C_3H_3^+$, and propargyl cation, l-$C_3H_3^+$ were computed using the Gaussian 03 suite of programs [30]. In a first step we optimized the geometries by second order perturbation theory (MP2). These calculations yielded a good description of the reaction path for both channels, including the transition state geometries. Subsequently a vibrational frequency analysis was performed at all stationary points, again at the MP2 level. In order to achieve a higher accuracy in the determination of the activation barriers, we carried out single point CCSD(T) coupled cluster calculations at the MP2 optimized geometries for all stationary points. The MP2 frequencies were employed in calculations of the zero point energies. In addition we carried out DFT calculations using the B3LYP functional. In all computations the 6-311^{++}G** basis set supplied by the Gaussian program was used.

4. Results and discussion

In Fig. 1a photoionization mass spectrum of allyl iodide (C_3H_5I) is depicted with the pyrolysis source turned on, using a photon energy of 10.55 eV. Beside the allyl-signal at $m/z = 41$ an equally large signal at $m/z = 39$ appears above 10 eV, due to dissociative photoionization to cyclopropenyl cation plus molecular hydrogen:

$$C_3H_5 + h\nu \rightarrow \text{c-}C_3H_3^+ + H_2 \qquad \Delta_R H^\circ(298\,\text{K}) = 9.42\,\text{eV} \tag{1}$$

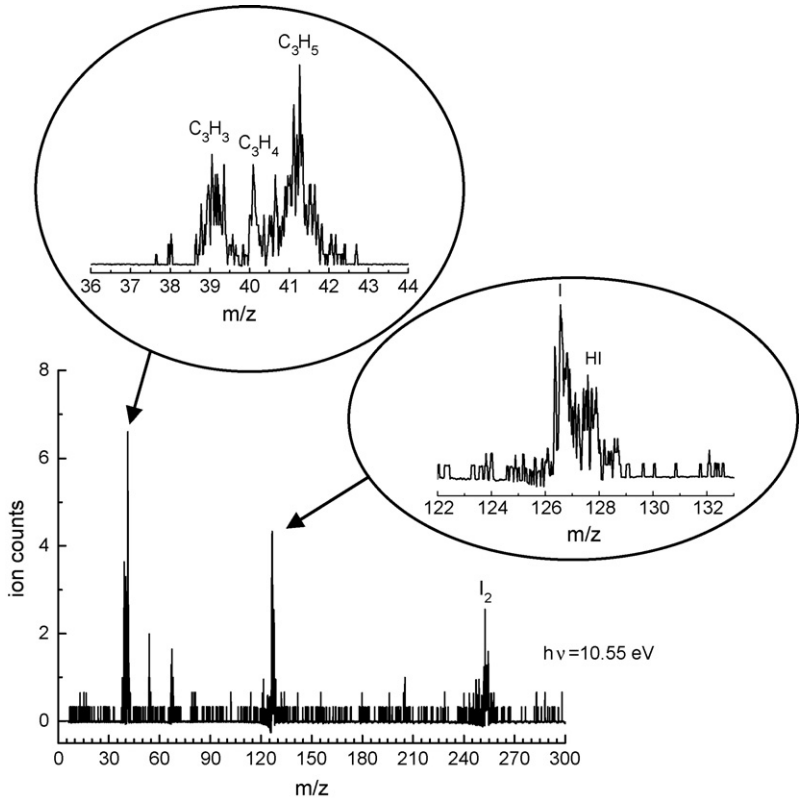

Fig. 1. The time-of-flight mass spectrum of pyrolyzed C_3H_5I at 10.55 eV, accumulated for 1200 s. A closer inspection of the spectrum indicates the presence of additional peaks at $m/z = 40$ (C_3H_4) and 128 (HI) that originate from bimolecular reactions in the pyrolysis nozzle.

The alternative reaction forming propargyl cation:

$$C_3H_5 + h\nu \rightarrow \text{l-}C_3H_3^+ + H_2 \qquad \Delta_R H^\circ(298\,\text{K}) = 10.45\,\text{eV} \tag{2}$$

lies energetically higher, but our computations discussed below indicate that contributions of this channel are possibly important at higher energies. A signal at $m/z = 40$ (allene cation) originates from a bimolecular radical–radical reaction (3) in the pyrolysis source:

$$C_3H_5 + I \rightarrow C_3H_4 + HI \tag{3}$$

as confirmed by the absence of this peak in experiments using hexadiene as the precursor (cf. Fig. 2). An inspection of the region around the I^+ signal shows contributions from HI^+ at $m/z = 128$ as well, further confirming this explanation. In addition a peak at the mass of I_2 is present, due to a radical–radical recombination reaction. Two more peaks can be identified at $m/z = 67$ and 54, corresponding to $C_5H_7^+$ and $C_4H_6^+$. They originate from the dissociative photoionization of hexadiene (see below) and indicate the recombination of two allyl units with subsequent fragmentation to be another bimolecular reaction pathway. The formation of side products can be significantly reduced by lowering the pyrolysis temperature albeit at the cost of a lower overall conversion efficiency. Bimolecular reaction products do generally not show up in laser experiments because the early part of the gas pulse is probed. Radicals accumulate during the gas pulse in the nozzle, initiating side reactions [31]

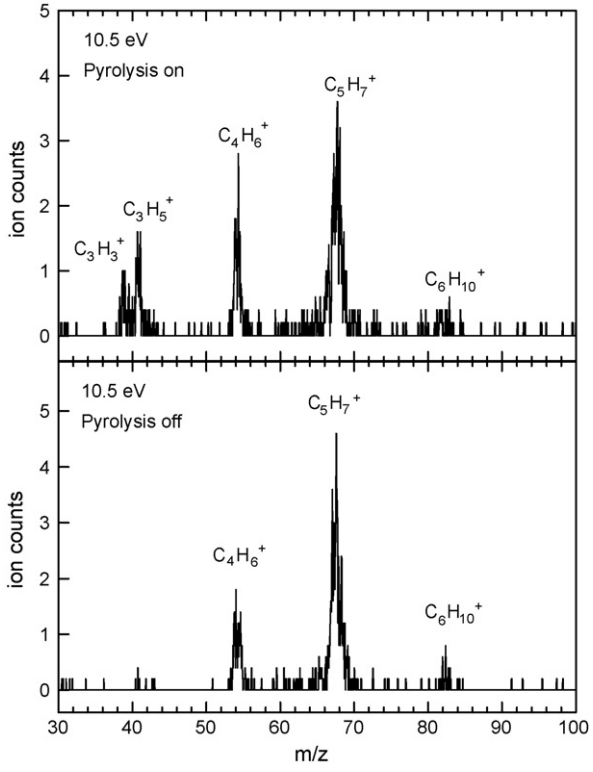

Fig. 2. The time-of-flight mass spectra of hexadiene, C_6H_{10}, recorded at a photon energy of 10.5 eV, with the pyrolysis source turned on (upper trace) and off (lower trace). Spectra were also accumulated for 1200 s.

that are easily monitored with the quasi-continuous synchrotron light. Although the spectrum in Fig. 1 was accumulated for 1200 s, the count numbers are rather small. A total of some 200 ions has been detected at $m/z = 41$, the signal at $m/z = 39$, originating exclusively from allyl through reaction (1), being comparable. Since the ionization cross-section of allyl is around 6 Mb [17], the photon flux in 24-bunch mode is 3×10^{10} photons/s on a roughly 1 mm^2 spot size [28], and the detection efficiency is assumed to be 30–50%, we estimate 2×10^5 allyl radicals/s in the ionization region. We thus conclude that the average radical density at the source exit is approximately two orders of magnitude smaller than in ns-laser experiments.

Experiments with the alternative precursor hexadiene (C_6H_{10}) provide a control for data interpretation [32]. Fig. 2 depicts mass spectra recorded at a photon energy of 10.5 eV. Already without pyrolysis (lower trace) fragment peaks at $m/z = 54$ ($C_4H_6^+$, presumably butadiene) and 67 ($C_5H_7^+$) are visible, indicating a significant amount of dissociative photoionization at this energy. The threshold for the appearance of $C_5H_7^+$, AE($C_5H_7^+$, C_6H_{10}), is known to be 9.35 eV [33], while the appearance energy of $C_4H_6^+$formation, AE($C_4H_6^+$, C_6H_{10}) was determined by us to lie between 10.5 and 11 eV. $C_3H_5^+$ appeared above 11.25 eV (literature value AE($C_3H_5^+$, C_6H_{10}) > 10.9 eV [34]) and no $C_3H_3^+$ is visible. When the pyrolysis source is turned on (upper trace) reaction (1) is observed. Note the absence of the signal at $m/z = 40$. Another interesting feature is the increase of the $C_4H_6^+$ signal at $m/z = 54$ upon pyrolysis, indicating the pyrolytic reaction $C_6H_{10} \rightarrow C_4H_6 + C_2H_4$, most likely butadiene plus ethylene. Due to reaction (4) [35]:

$$C_4H_6 + h\nu \rightarrow C_3H_3^+ + CH_3 \qquad AE = 11.4\,eV \qquad (4)$$

a second independent channel for the formation of ions at $m/z = 39$ is thus available. Compared to allyl iodide, hexadiene is therefore less suited to investigate the VUV-photochemistry of allyl. The VUV-photochemistry of hexadiene itself was investigated in great detail and will be discussed in a forthcoming publication (Alcaraz, Elhanine, in preparation).

Fig. 3 depicts the signal ratios $(m/z = 39)/(m/z = 39 + m/z = 41)$ and $(m/z = 41)/(m/z = 39 + m/z = 41)$ as a function of photon energy. The data points were obtained from experiments using C_3H_5I as the precursor. At selected energies spectra have been repeatedly recorded over a period of several hours. The resulting scatter of the data is partly due to the small ion count numbers (cf. Figs. 1 and 2), partly a measure of the long-term stability of the setup. A signal from $C_3H_3^+$ (solid squares) due to dissociative reaction (1) appears above $h\nu = 10$ eV. Around 10.45 eV the $C_3H_3^+$signal has increased to 50% of the level observed above 11 eV, which can serve as an approximated appearance energy. Interestingly a significant signal at the mass of allyl (open squares) is still present in the spectrum at higher photon energies, although the intensity of the $C_3H_3^+$ signal has reached a constant level. There are two possible reasons for the presence of allyl cation at higher photon energies:

(a) Dissociative photoionization of unpyrolyzed precursor molecules can contribute to the signal. In our experiments on ethyl and propargyl [23] this channel was responsible for a significant part of the signal. Since the appearance energy for this process in allyl iodide, AE($C_3H_5^+$, C_3H_5I) is 9.8 eV [36], the conversion efficiency can only be checked between 9.3 eV (IE of C_3H_5I) and 9.8 eV. In most experiments we achieved an almost complete conversion of allyl iodide, but some showed a small residual signal at the mass of the precursor. Although a contribution of this reaction to the signal is expected to be considerably smaller than in the recent experiments on ethyl and propargyl [23], it cannot be ruled out completely.

(b) In later experiments we observed some electron counts without the synchrotron beam. This background signal went away when the pyrolysis source was turned off, and is thus due to electrons formed in the pyrolysis tube. These electrons cause false coincidences that are not taken into account in our correction procedure.

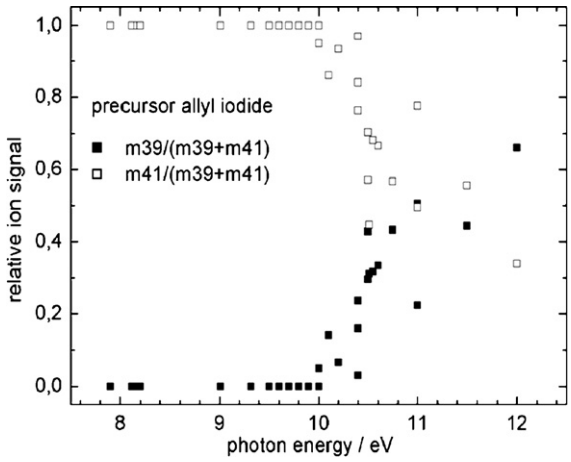

Fig. 3. Dissociative Photoionization of C_3H_5 as a function of photon energy. Formation of $C_3H_3^+$ sets in above 10 eV and reaches 50% of the maximum value between 10.4 and 10.5 eV. As visible the signal of the allyl cation does not disappear at higher photon energies, rendering a detailed analysis of the curve difficult. Note that measurements were repeated at selected photon energies.

To aid the data interpretation we carried out ab initio calculations on various levels of theory. The energies, calculated at the MP2, CCSD(T) and DFT level of theory and corrected for the zero point vibrational energy, are summarized in Table 1. They are given relative to the electronic energy of the allyl cation, which was chosen as the reference point. In Fig. 4 the intermediates on the reaction pathways leading from $C_3H_5^+$ to c-$C_3H_3^+$ and l-$C_3H_3^+$, both associated with formation of H_2 are given together with the CCSD(T) energies that we consider to be the most reliable. For the ease of comparison with the experimental data, the energies in the figure are given with respect to the ground state of the neutral allyl radical, assuming an ionization energy of 8.13 eV. All methods yield energies for the c-$C_3H_3^+ + H_2$ product channel that are in close agreement with the experimentally known standard heat of formation. The energy maximum along the reaction coordinate to c-$C_3H_3^+ + H_2$ is the transition state connecting the corner protonated cyclopropene intermediate with the products. Dissociative photoionization of

Table 1
Electronic energies for the stationary points along the reaction coordinate from allyl cation to cyclopropenyl cation and propargyl cation, calculated by various computational methods

Species	B3LYP	MP2	CCSD(T)	Ref. [37]
$C_3H_5^+$ (allyl cation)	0	0	0	0
TS1	+1.73	+1.52	+1.59	+1.69
c-$C_3H_5^+$ (corner prot.)	+1.21	+1.03	+1.13	+1.24
TS2	+2.59	+2.40	+2.54	+2.68
c-$C_3H_3^+ + H_2$	+1.31	+1.06	+1.19	+1.21
TS3	+1.21	+1.23	+1.21	
$C_3H_5^+$ (2-propenyl)	+0.26	+0.41	+0.37	+0.45
TS4	+2.47	+2.74	+2.64	+2.84
l-$C_3H_3^+ + H_2$	+2.34	+2.37	+2.32	+2.40

All energies are given in eV relative to the ground state of the allyl cation.

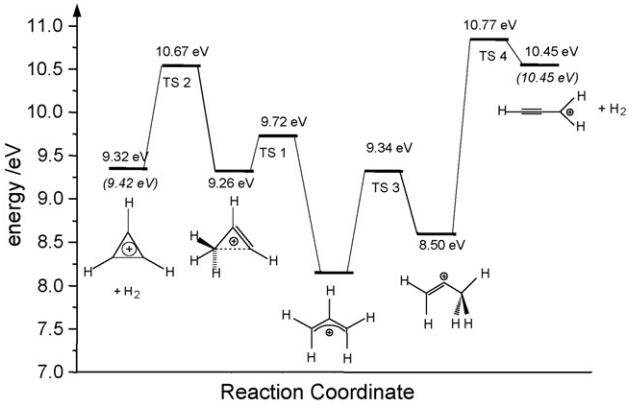

Fig. 4. Computed reaction coordinate for the pathways for dissociation of the allyl cation with the CCSD(T) energies for the stationary points. The experimental $\Delta_f H^\circ$ (298 K) for the product channels are given in italics. Although the c-$C_3H_3 + H_2$ product channel is energetically most favorable, the barrier to l-$C_3H_3^+ + H_2$ is only higher by 0.1 eV.

allyl will occur when the photon energy suffices to overcome this barrier. CCSD(T) calculations place it at 10.67 eV, at the MP2 level it is slightly lower (10.53 eV). We also investigated the channel (2), leading to the propargyl cation. In the earlier computations [37] the barrier to formation of propargyl cation was computed to lie around 11 eV, but our own CCSD(T) calculations yielded a lower transition state energy of around 10.77 eV. Since the TS4 is less rigid than TS2, it has to be considered as a competing reaction channel. We carried out RRKM calculations [38] employing the barriers given in Fig. 4 and the frequencies from MP2 computations scaled by 0.94, as summarized in Table 2. A reaction path degeneracy of 2 was assumed because the allyl cation has C_{2v} symmetry, whereas the transition states have C_s (TS2) and C_1 (TS4) symmetry respectively. Transition states TS1 and 3 were neglected because of their much lower energy.

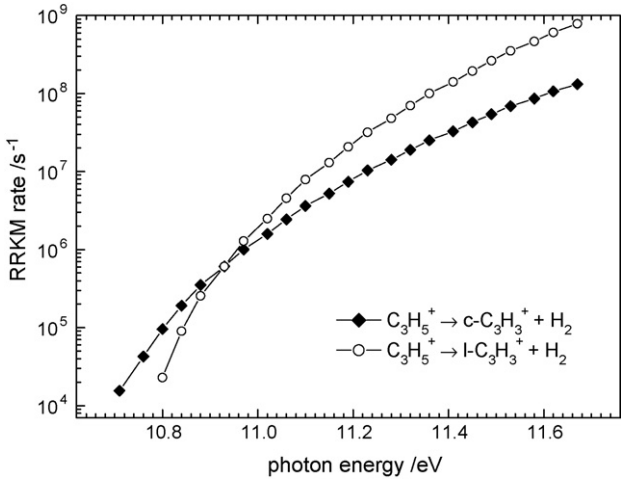

Fig. 5. RRKM-rates for the two dissociation pathways of the allyl cation, leading to c-$C_3H_3^+ + H_2$ and l-$C_3H_3^+ + H_2$. Only close to threshold does the former channel dominate.

The orbiting transition state for the l-$C_3H_3^+ + H_2$ channel was also considered not important. The results are depicted in Fig. 5. As visible the reaction rates become similar around 10.9 eV. Thus only in the region of the dissociation threshold will formation of the thermochemically most stable product c-$C_3H_3^+$ dominate. Above 11 eV the l-$C_3H_3^+ + H_2$ channel will be kinetically favored. Interestingly Zhang et al. [18] pointed out that the PIE-spectra of propargyl obtained in flames might have contributions from dissociative ionization of larger radicals. Our work indicates dissociative ionization of allyl as a possible source for such a contribution. The authors of the earlier computational study on the reactions leading to $C_3H_3^+$ examined the reaction of methyl cation with acetylene that proceeds via various intermediates on the $C_3H_5^+$ potential energy surface [37]. They identified most of the critical structures relevant to us by MP2 and optimized them on the MP4 level of theory, using a 6-31G** basis. Their results are also given in Table 1 for comparison. As shown, their energies are quite similar to the ones obtained by us. However, they calculate somewhat higher energies for the transition states.

Although a detailed analysis of the data summarized in Fig. 3 is difficult, our results are in good agreement with the available literature data. The appearance energy of $C_3H_3^+$ generated from allyl AE($C_3H_3^+$, C_3H_5) was determined by electron impact mass spectrometry to be around 10.48 eV [39]. Since the constant level of allyl cation at high photon energies complicates the evaluation of an accurate appearance energy in our experiments, this value of 10.48 eV should be compared to the 50% value of 10.45 eV discussed above. Considering that the computed transition state energies of 10.67 and 10.53 eV at the CCSD(T)

Table 2
Vibrational wave numbers employed in the RRKM calculations, corresponding to the MP2 wave numbers scaled by a factor of 0.94

Stationary point	Vibrational wave numbers (cm^{-1})
$C_3H_5^+$	3093, 3090, 3058, 2983, 2982, 1564, 1477, 1380, 1247, 1230, 1060, 1059, 1000, 969, 904, 603, 420, 248
TS2	3285, 3147, 3102, 3055, 1581, 1400, 1324, 1158, 1041, 990, 923, 869, 854, 835, 676, 628, 597
TS4	3757, 3173, 3069, 2966, 1958, 1390, 1122, 1064, 983, 965, 728, 620, 594, 537, 429, 303, 247

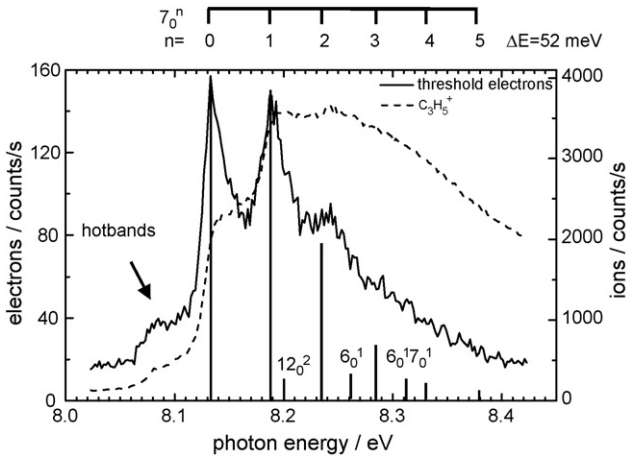

Fig. 6. Threshold photoelectron spectrum of C_3H_5. For comparison a stick spectrum based on Franck–Condon simulations is given, assuming in the cation a C–C bond length $r_{(C–C)} = 1.365$ Å and a CCC angle $\Theta_{CCC} = 117°$.

and MP2 levels of theory employed by us are accurate to within 0.1–0.2 eV, the agreement between experiment and calculation is also reasonable.

Structural information on the cations is available by threshold photoelectron spectroscopy (TPES). The TPE spectrum of allyl shown in Fig. 6 was recorded with a continuous molecular beam, using the 1,5-hexadiene precursor. The storage ring was operated in 24-bunch mode, thus no temporal discrimination was used. TPES taken either using allyl iodide as a precursor, or taken with a pulsed beam, or with temporal discrimination using the two-bunch mode, have a similar appearance. The spectral structure resembles the one observed in earlier conventional photoelectron spectra [40], but at a higher resolution. The figure also includes the signal recorded in the allyl mass channel, i.e., the photoionization efficiency (PIE) curve. As visible, several peaks in the TPE spectrum are associated with distinct steps in the PIE spectrum. We analyzed the TPES performing a Franck–Condon simulation, following the approach outlined in the literature [31]. A starting geometry for the ion was obtained from MP2 calculation with a 6-31G** basis set, which was then refined to achieve a good fit to the spectrum. For the neutral ground state the geometries derived from IR laser diode spectroscopy were used [41]. Other parameters necessary for the Franck–Condon simulations, like force constants and atomic displacement matrices, were also obtained from the ab initio calculations. In Fig. 6 the threshold photoelectron spectrum is shown with the best stick spectrum given for comparison. Changes in the CCC bond angle Θ_{CCC} and C–C bond length $r_{(C–C)}$ had a pronounced effect on the spectrum. The stick spectrum, given in the bottom trace of the figure, was obtained with $r_{(C–C)} = 1.365$ Å and $\Theta_{CCC} = 117°$ for the cation instead of the ab initio values of $r_{(C–C)} = 1.3826$ Å and $\Theta_{CCC} = 117.6°$. All other parameters were fixed at the ab initio values of 1.0802 Å (central C–H bond), 1.0824 Å (C–H exo), 1.0836 Å (C–H endo), 121.7° (CCH exo) and 120.78° (C–H endo). No significant geometry change along these coordinates is expected. The vibrational wave numbers were taken from Ref. [32]. In the neutral electronic ground state the corresponding geometry parameters are $\Theta_{CCC} = 123.96°$ and $r_{(C–C)} = 1.3869$ [42]. The geometry change upon ionization leads to significant vibrational activity in the CCC bending mode ν_7^+ (431 cm^{-1}). Some activity in ν_6^+ (CCC stretch, 1080 cm^{-1}) and ν_{12}^+ (symmetric CH_2 twist) is also expected, but cannot be resolved in the experiment. In addition contributions from hot and/or sequence bands are visible on the low energy side of the spectrum. In an earlier paper we derived an ionic geometry by simulating picosecond time-resolved photoelectron spectra from the C 0_0^0 state [42], i.e., from a different initial state, obtaining the best fit with $r_{(C–C)} = 1.37$ Å and $\Theta_{CCC} = 116°$ for the cation. However, in the ps-experiments the force constants and atomic displacement matrices of the C-state were taken from neutral ground state computations. We therefore believe that the simulation presented in Fig. 6 is more accurate, but in good agreement with the previous one.

We deduced an ionization energy of 8.13 ± 0.01 eV, in agreement with the ionization energies of 8.13 eV determined by conventional photoelectron spectroscopy [40] and by extrapolation of s-Rydberg series [43], but deviating from the value of 8.153 eV determined by [1 + 1′] ZEKE-spectroscopy through various intermediate states [44]. Possible reasons for this discrepancy are the neglect of the rotational structure and hot- or sequence band contributions to the spectrum. Note that the half-width of the peaks is larger than the 10 meV optimum resolution, indicating a radical beam that has a considerable internal energy. Since we are sampling all parts of the molecular beam the vibrational temperature is higher than the ≈100 K typically achieved in laser experiments. We plan to carry out one-photon ZEKE-experiments using VUV lasers to further elucidate the reasons for the discrepancies. Computed ionization energies depend strongly on the method and basis set used. Using DFT calculations with a B3LYP functional, we calculated IE = 8.14 eV, within the range of the available experimental values. MP2 (IE = 7.66 eV) and CCSD(T) (IE = 7.91 eV) computations resulted in substantially lower values. Recent highly accurate ab initio calculations [45] arrived at an IE(C_3H_5) of 8.158 eV, thus very close to the ZEKE value. The authors were also able to reproduce the measured ionization energies of CH_2, CH_3 and C_3H_3 to within a few millielectronvolts. For C_2H and for radicals with nonclassical cations the experimental IE's are probably not well enough known for a comparison.

5. Summary and conclusion

The dissociative photoionization of the allyl radical C_3H_5 was studied using synchrotron radiation for photoexcitation. Allyl was produced by supersonic jet flash pyrolysis from allyl iodide and 1,5-hexadiene respectively. Under the quasi-continuous source conditions bimolecular processes could not be suppressed, leading to additional side products. The dissociative photoionization of allyl leads to $C_3H_3^+ + H_2$. The process sets in above 10 eV. The $C_3H_3^+$ signal reaches 50% of its constant high energy level around 10.45 eV, in good agreement with an earlier AE of 10.48 eV determined by mass spectrometry. On thermochemical grounds cyclopropenyl cation, c-$C_3H_3^+$, is expected to be the dominant product at the appearance threshold. Coupled cluster calculations yielded barriers of 10.77 eV to the l-

$C_3H_3^+ + H_2$ channel and 10.67 eV to the c-$C_3H_3^+ + H_2$ channel. A further RRKM study indicates that due to the larger number of low-frequency vibrations formation of propargyl cation, l-$C_3H_3^+$, becomes competitive already at small excess energies. The threshold photoelectron spectrum of the allyl radical shows considerable activity in the CCC bending vibration. A Franck–Condon analysis yielded a C–C bond length of 1.365 Å and a CCC angle of 117° for the cationic geometry.

Acknowledgements

This work was supported by the Deutsche Forschungsgemeinschaft under contracts Fi575/3-1 and 3-3. Travel subsidies were provided by LURE through the European Commission programme "Transnational access to research infrastructures", by the German/French binational PROCOPE program and by the BFHZ. We would like to thank the staff at LURE for operating the Super-ACO storage ring and for technical support on the SU5 beamline, in particular Bertrand Pilette and Laurent Nahon.

References

[1] A. Dalgarno, J.L. Fox, in: C.Y. Ng, T. Baer, I. Powis (Eds.), Unimolecular and Bimolecular Reaction Dynamics, John Wiley & Sons, Chichester, 1994.
[2] C.N. Keller, V.G. Anicich, T.E. Cravens, Planet. Space Sci. 46 (1998) 1157.
[3] P.R. Mahaffy, Science 308 (2005) 969.
[4] T. Owen, Nature 438 (2005) 756.
[5] http://www.saturn.jpl.nasa.gov/multimedia/images/image-details.cfm?imageID=1498, Ion mass spectrum of Titan upper atmosphere, 2005.
[6] T.A. Cool, K. Nakajima, T.A. Mostefaoui, F. Qi, A. McIlroy, P.R. Westmoreland, M.E. Law, L. Poisson, D.S. Peterka, M. Ahmed, J. Chem. Phys. 119 (2003) 8356.
[7] C.A. Taatjes, S.J. Klippenstein, N. Hansen, J.A. Miller, T.A. Cool, J. Wang, M.E. Law, P.R. Westmoreland, Phys. Chem. Chem. Phys. 7 (2005) 806.
[8] N. Hansen, S.J. Klippenstein, C.A. Taatjes, J.A. Miller, J. Wang, T.A. Cool, B. Yang, R. Yang, L. Wei, C. Huang, J. Wang, F. Qi, M.E. Law, P.R. Westmoreland, J. Phys. Chem. A 110 (2006) 3670.
[9] J.D. Barr, A. De Fanis, J.M. Dyke, S.D. Gamblin, N. Hooper, A. Morris, S. Stranges, J.B. West, T.G. Wright, J. Chem. Phys. 110 (1999) 345.
[10] J. Eberhard, W.-C. Chen, C.-H. Yu, Y.P. Lee, B.-M. Cheng, J. Chem. Phys. 108 (1998) 6197.
[11] J.B. West, J.M. Dyke, A. Morris, T.G. Wright, S.D. Gamblin, J. Phys. B: Atom. Mol. Opt. Phys. 32 (1999) 2763.
[12] J.D. Barr, L. Beeching, A. De Fanis, J.M. Dyke, S.D. Gamblin, N. Hooper, A. Morris, S. Stranges, J.B. West, A.E. Wright, T.G. Wright, J. Electron Spectrosc. Relat. Phenom. 108 (2000) 47.
[13] J.A. Mueller, B.F. Parsons, L.J. Butler, F. Qi, O. Sorkhabi, A.G. Suits, J. Chem. Phys. 114 (2001) 4505.
[14] T. Schüßler, H.-J. Deyerl, S. Dümmler, I. Fischer, C. Alcaraz, M. Elhanine, J. Chem. Phys. 118 (2003) 9077.
[15] C.A. Taatjes, D.L. Osborn, T.A. Cool, K. Nakajima, Chem. Phys. Lett. 394 (2004) 19.
[16] J.C. Robinson, N.E. Sveum, D.M. Neumark, J. Chem. Phys. 119 (2003) 5311.
[17] J.C. Robinson, N.E. Sveum, D.M. Neumark, Chem. Phys. Lett. 383 (2004) 601.
[18] T. Zhang, X.N. Tang, K.-C. Lau, C.Y. Ng, C. Nicolas, D.S. Peterka, M. Ahmed, M.L. Morton, B. Ruscic, R. Yang, L.X. Wei, C.Q. Huang, B. Yang, J. Wang, L.S. Sheng, Y.W. Zhang, F. Qi, J. Chem. Phys. 124 (2006) 074302.
[19] J. Berkowitz, C.A. Mayhew, B. Ruscic, J. Chem. Phys. 88 (1988) 7396.
[20] B. Ruscic, J. Berkowitz, J. Chem. Phys. 95 (1991) 4033.
[21] J. Berkowitz, E. Rühl, H. Baumgärtel, in: U. Becker, D.A. Shirley (Eds.), VUV and Soft X-ray Photoionization, Plenum Press, New York, 1996.
[22] B. Ruscic, M. Litorja, Chem. Phys. Lett. 316 (2000) 45.
[23] T. Schüßler, W. Roth, T. Gerber, I. Fischer, C. Alcaraz, Phys. Chem. Chem. Phys. 7 (2005) 819.
[24] T. Baer, P.-M. Guyon, in: C.Y. Ng, T. Baer, I. Powis (Eds.), High Resolution Laser Photoionisation and Photoelectron Studies, Wiley, New York, 1995.
[25] R. Atkinson, J. Arey, Acc. Chem. Res. 31 (1998) 574.
[26] A. Webster, Mon. Not. R. Astron. Soc. 265 (1993) 421.
[27] M. Richard-Viard, A. Delboulbe, M. Vervloet, Chem. Phys. 209 (1996) 159.
[28] L. Nahon, C. Alcaraz, J.L. Marlats, B. Lagarde, F. Polack, R. Thissen, D. Lepere, K. Ito, Rev. Sci. Instrum. 72 (2001) 1320.
[29] D.W. Kohn, H. Clauberg, P. Chen, Rev. Sci. Instrum. 63 (1992) 4003.
[30] M.J. Frisch, G.W. Trucks, H.B. Schlegel, G.E. Scuseria, M.A. Robb, J.R. Cheeseman, J. Montgomery, J.A.T. Vreven, K.N. Kudin, J.C. Burant, J.M. Millam, S.S. Iyengar, J. Tomasi, V. Barone, B. Mennucci, M. Cossi, G. Scalmani, N. Rega, G.A. Petersson, H. Nakatsuji, M. Hada, M. Ehara, K. Toyota, R. Fukuda, J. Hasegawa, M. Ishida, T. Nakajima, Y. Honda, O. Kitao, H. Nakai, M. Klene, X. Li, J.E. Knox, H.P. Hratchian, J.B. Cross, C. Adamo, J. Jaramillo, R. Gomperts, R.E. Stratmann, O. Yazyev, A.J. Austin, R. Cammi, C. Pomelli, J.W. Ochterski, P.Y. Ayala, K. Morokuma, G.A. Voth, P. Salvador, J.J. Dannenberg, V.G. Zakrzewski, S. Dapprich, A.D. Daniels, M.C. Strain, O. Farkas, D.K. Malick, A.D. Rabuck, K. Raghavachari, J.B. Foresman, J.V. Ortiz, Q. Cui, A.G. Baboul, S. Clifford, J. Cioslowski, B.B. Stefanov, G. Liu, A. Lias-henko, P. Piskorz, I. Komaromi, R.L. Martin, D.J. Fox, T. Keith, M.A. Al-Laham, C.Y. Peng, A. Nanayakkara, M. Challacombe, P.M.W. Gill, B. Johnson, W. Chen, M.W. Wong, C. Gonzalez, J.A. Pople, Gaussian 03 Revision B04, Gaussian Inc., Pittsburgh, PA, 2003.
[31] P. Chen, in: I. Powis (Ed.), Unimolecular and Bimolecular Reaction Dynamics, Wiley, New York, 1994, p. 371.
[32] I. Fischer, P. Chen, J. Phys. Chem. A 106 (2002) 4291.
[33] P. Wolkoff, J.L. Holmes, F.P. Lossing, Can. J. Chem. 58 (1980) 251.
[34] P.J. Hart, H.R. Friedli, Chem. Commun. (1970) 621.
[35] A.C. Parr, F.A. Elder, J. Chem. Phys. 49 (1968) 2659.
[36] J.C. Traeger, Int. J. Mass Spectrom. Ion Process. 58 (1984) 259.
[37] R. Lopez, J.A. Sordo, T.L. Sordo, P.V.R. Schleyer, J. Comp. Chem. 17 (1996) 905.
[38] W.L. Hase, D.L. Bunker, M. Sullivan, QCPE 11 (1975) 291.
[39] F.P. Lossing, J.L. Holmes, J. Am. Chem. Soc. 106 (1984) 6917.
[40] F.A. Houle, J.L. Beauchamp, J. Am. Chem. Soc. 100 (1978) 3290.
[41] E. Hirota, C. Yamada, M. Okunishi, J. Chem. Phys. 97 (1992) 2963.
[42] T. Schultz, I. Fischer, J. Chem. Phys. 109 (1998) 5812.
[43] C.-W. Liang, C.-C. Chen, C.-Y. Yin Wei, Y.-T. Chen, J. Chem. Phys. 116 (2002) 4162.
[44] T. Gilbert, I. Fischer, P. Chen, J. Chem. Phys. 113 (2000) 561.
[45] K.-C. Lau, C.Y. Ng, J. Chem. Phys. 122 (2005) 224310.